Engineering Multiscale Heterostructure as Ionic Diode and Light-Driven Ion Pump for Osmotic-Solar Energy Harvesting

Xinyue Zhang[1,2], Baohu Wu[3], Huiqing Wu[1,2*] & Peiyi Wu[1,2*]

[1]Key Laboratory of Science & Technology of Eco-Textile, Ministry of Education, College of Chemistry and Chemical Engineering, Donghua University, Shanghai 201620, [2]National Innovation Center of Advanced Dyeing and Finishing Technology, Tai'an, Shandong 271000, [3]Jülich Centre for Neutron Science (JCNS), Heinz Maier-Leibnitz Zentrum (MLZ), Forschungszentrum Jülich, 85748 Garching

**Corresponding authors: wupeiyi@dhu.edu.cn; Huiqingwu@dhu.edu.cn*

As blue energy, osmotic power holds tremendous potential for electricity generation via membrane-based reverse electrodialysis. However, current processes suffer from low energy output mainly due to inadequate transmembrane ion transport and a polarization phenomenon. Inspired by plant growth and photosynthesis, we proposed a robust heterogeneous membrane that enabled ionic-diode rectified and light-enhanced ion transport for efficient osmotic-solar energy harvesting. The membrane was rationally constructed by in-situ growth of polyaniline (PANI) onto a sulfonated matrix, creating a multiscale heterostructure that enabled the coexistence of a Janus-like architecture and semiconductor heterojunction. Benefiting from multi-asymmetries of geometry, charge, and chemistry, the membrane delivered a high unidirectional ion flow and suppressed polarization, generating an exceptional osmotic power density of up to 12.6 W m^{-2} at a 50-fold salinity gradient. Light-driven ion pumping was achieved by the synergistic photothermal and photoelectric effect of PANI heterojunction. Under light irradiation, temperature gradient and transmembrane potential were triggered simultaneously, accelerating ion movement, thereby elevating the energy conversion output. This work pioneers the development of high-performance power generators capable of harnessing energy from diverse salty sources coupled with a solar resource.

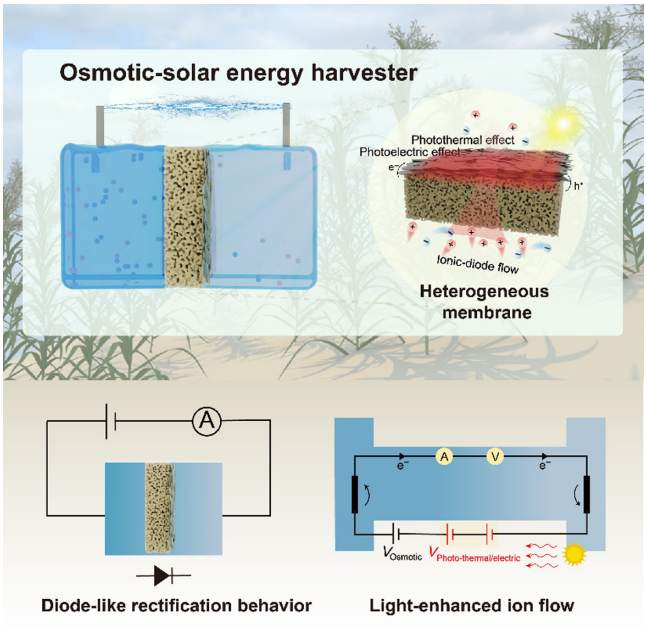

Keywords: heterostructure, salinity gradient, ionic diode, light-driven, osmotic power, solar energy

Introduction

The depletion of fossil fuels and the exacerbation of the environmental crisis have intensified the need for abundant, renewable, and inexpensive energy sources worldwide. Osmotic energy, derived from saline resources such as seawater, brines, and wastewater, is being intensively explored as a potential solution.[1] Membrane-based reverse electrodialysis (RED) offers an alternative avenue for harvesting osmotic power. This technique relies on semipermeable membranes that selectively drive ions pass through, generating a net current that can be directly converted into electricity. Various materials such as polymers, two-dimensional materials, and framework materials have been explored for membrane construction.[1-3] However, the current RED stacks are in their infancy and suffer from several critical limitations.[4] For example, the trade-off between permeability and selectivity is always a challenge for membranes with sub-/nanoscale pores. While using ultrathin membranes to improve transmembrane permeance is an alternative, there is a shortage of robust materials and scaled-up manufacture. Energy loss induced by concentration polarization further deteriorates the conversion energy efficiency. Moreover, the osmotic output power density remains insufficient to meet the industrial benchmark of 5 W m^{-2}.

Heterogeneous membranes with distinct bilayers hold promise for enhancing the performance of RED devices. By independently tailoring the channel geometry and charge polarity of each layer, these membranes can synergistically achieve asymmetric properties, enabling efficient ion rectification behavior. This ionic-diode effect facilitates unidirectional ion transport, alleviating the polarization phenomenon, significantly reducing the dissipation of Gibbs free energy, and ultimately boosting the energy conversion efficiency. So far, different types of heterogeneous membranes, including combinations of organic/organic, inorganic/inorganic, and organic/inorganic constituents, have been explored. Also, several fabrication methods have been employed, including surface modification, spinning coating, reaction-diffusion, electrodeposition, sequence filtration, layer-by-layer deposition, functionalization transfer, microwave-assisted growth, and so on.[5-15] Besides, a dense layer with high charge density serves as the primary barrier, controlling selective ion transport. Meanwhile, the other relatively loose layer generally works as an asymmetric functional layer, facilitating one-way ion flow. However, regarding the current heterostructures of the membranes, there are still some tricky issues to be addressed. For example, the incompatible interface or weak interfacial bonding may trigger the delamination and damage of the dual layers. The high interfacial resistance may deteriorate the transmembrane ion transport. The scanty function of the loose layer brings about the limited enhancement of the membrane performance.

Moreover, external factors such as light, heat, force, and chemical reactions have also been used to pursue the enhancement of ion migration.[16-26] Light, in particular, offers a unique advantage in augmenting osmosis energy harvesting. The abundance of natural sunlight can be harnessed and integrated into nanofluidic systems for industrial applications. The remarkable efficiency of light-driven ion transport often arises from a complex interplay of mechanisms involving photoelectric, photothermal, and photochemical effects, based on photoresponsive materials inside the membrane.[27] Crucially, a deliberately constructed heterojunction within the heterogeneous membrane, can facilitate electron-hole separation and promote confined ion diffusion, leading to light-enhanced energy output.[28-32] Thus, strategically creating selective and functional layers of heterogeneous membrane that combines ionic-diode rectification and light regulation for ion transport is highly desired for maximizing energy conversion output. However, the exquisite design and flexible construction of heterogeneous architectures that could optimize both interfacial ion movement and light-triggered ion transport are urgently in demand but challenging, as they are essential for developing efficient osmotic-solar energy conversion systems.

Our design principles for high-performance heterogeneous membranes are plant-inspired. Drawing inspiration from plant sowing and growing, a stable heterostructure was constructed in-situ. Moreover, we integrated light energy into the system for energy conversion, analogous to the photosynthetic process in plants. Therefore, we developed a delicate heterostructure, consisting of sulfonated poly(2,6-dimethyl-1,4-phenylene oxide) (SPPO) matrix and in-situ deposited polyaniline (PANI) layer, for the high-efficiency osmotic-solar energy conversion system. The designed SPPO/PANI heterostructure offered several advantages as follows: (1) A robust multiscale heterostructure was facilely achieved, where the negatively-charged dense SPPO matrix and loose PANI layer serve as the screening layer and functional layer, respectively. This combination resulted in inherent high ion conductivity and selectivity, along with good mechanical strength and excellent stability. (2) The heterostructure, characterized by geometrical, charge, and chemical asymmetries, facilitated one-way ion diffusion and suppressed polarization phenomenon, achieving a stable ionic diode effect and enhancing osmotic energy conversion efficiency. (3) Under light irradiation, the output power density increased significantly due to the synergistic photothermal and photoelectric effect of PANI heterojunction. The PANI layer efficiently converted light to heat, creating a temperature gradient that drove ion migration. Simultaneously, the elaborate heterojunction built within SPPO/PANI

accelerated the transfer of photoinduced carriers and suppressed their recombination, promoting spontaneous ion flow in nanofluidic channels.

As a proof-of-concept, this work pioneers a robust strategy for multiscale heterostructure construction, presenting a highly promising device for sustainable power generation from osmotic energy and solar energy. Under a 50-fold salinity gradient, the system delivers a maximum osmotic power density of 12.6 W m^{-2}, far surpassing both commercial benchmarks and state-of-the-art membranes. With light irradiation, the osmotic output power density could increase to 14.6 W m^{-2}. An impressive osmotic power output of up to 19.6 W m^{-2} is produced by mixing industrial dyeing residual wastewater and natural river water, offering exciting possibilities for sustainable energy production even from waste streams.

Experimental Methods

Materials

Poly(2,6-dimethyl-1,4-phenylene oxide) (PPO) was supplied by the Institute of Chemical Engineering of Beijing, China. Rhodamine 6G and chloroform were obtained from Adamas-beta. Sulforhodamine, chlorosulfonic acid, and magnesium chloride ($MgCl_2$) were bought from Shandong Yousuo Chemical Technology, Jiuding Chemistry, and Bide Pharmatech Co., Ltd., Shanghai, China, respectively. Ammonium persulfate (APS), sodium chloride (NaCl), sodium hydroxide (NaOH), and hydrochloric acid (HCl) were purchased from Sinopharm. Co., Ltd., Shanghai, China. Aniline (ANI), lithium chloride (LiCl), and dimethyl sulfoxide (DMSO) were purchased from Aladdin Biochemical Technology, Co., Ltd., Shanghai, China. Calcium chloride ($CaCl_2$) and potassium chloride (KCl) were received from Shanghai Macklin Co., Ltd., China. All the chemicals were used without further purification, and deionized (DI) water was used in all experiments.

Synthesis of SPPO

First, SPPO was prepared by sulfonation of PPO using chlorosulfonic acid according to the literature.[33] PPO (2 g) was dissolved in chloroform (30 mL) to obtain a uniform PPO solution (5%). Under stirring, 2 g of chlorosulfonic acid/chloroform solution (6%) was added dropwise to the PPO solution. When precipitation occurred, the reaction was terminated. Then the precipitate (SPPO) was removed, washed with deionized (DI) water to neutrality, and dried. The degree of sulfonation of the obtained SPPO was calculated to be 81.2% from proton nuclear magnetic resonance (^{1}H NMR) measurement (AVANCE NEO, Zurich, Switzerland).

Preparation of SPPO and SPPO/PANI membrane

A homogeneous casting solution (~10 wt %) was prepared by dissolving SPPO in DMSO. The solution was then cast on the glass plate with a doctor blade of 100 μm, and the cast-glass plate was kept in an oven at 80 °C for 6 h. The SPPO membrane was finally obtained.

The in-situ PANI growth on the SPPO membrane was operated as follows: First, the as-prepared SPPO membrane was tightly placed on the glass sheet to ensure the growth of the PANI layer only on one side of the SPPO. The SPPO membrane with glass sheet was immersed in a solution containing 0.01 M ANI and 1 M HCl, allowing sufficient absorption of ANI monomer on the SPPO surface. The polymerization was initiated by adding APS (0.005 M) and carried on for 3 h under stirring in the ice bath. The process was determined to be once-through PANI growth on SPPO. For a repetitive polymerization process, the above SPPO/PANI membrane obtained was immersed into an ANI/HCl mixture and the PANI polymerization was excited in succession again. The resulting final SPPO/PANI membrane was washed thoroughly with DI water.

Characterizations

^{1}H NMR spectra were recorded on an AVANCE NEO instrument (Zurich, Switzerland). Fourier transform infrared (FT-IR) spectra were obtained from a Nicolet-iS50 spectrometer (Thermo Fisher Scientific, Massachusetts, United States) with attenuated total reflectance (ATR) accessories. A scanning electron microscopy (SEM, SU8230, Hitachi) was employed for membrane morphology and structural observation. The ζ-potential values of the membranes were obtained from the SurPASS3 instrument (Anton Paar, Graz, Austria) using 1 mM KCl as the electrolyte solution at pH 2–12. The hydrophilicity of the membranes was measured using a contact angle tester (XG-CAMC3; Xuanzhun Co., Ltd, Shanghai, China). Low-field nuclear magnetic resonance (LF-NMR; VTMR20-010V-I, Shanghai New-Mai Electronic Co., Ltd., China) was employed to study the molecular dynamics of water within the pore of the membrane. The transverse relaxation time (T_2) was measured using the Carre–Purcelle–Meiboome–Gill (CPMG) sequence with 0.5 T of magnetic field intensity. General tensile test and peeling test were carried out on a vertical dynamometer (ESM303, MARK-10, USA) with a straining rate of 20 mm/min. Thermogravimetric analysis (TGA) curve was recorded on a (NETZSCH TG 209F3, Bavaria, Germany) from room temperature to 600 °C in a nitrogen atmosphere at a heating rate of 20 °C/min. Electron paramagnetic resonance (EPR) test was performed on a Bruker A300 EPR spectrophotometer (Bruker, Karlsruhe, Germany), using 1–20 mW microwave power and

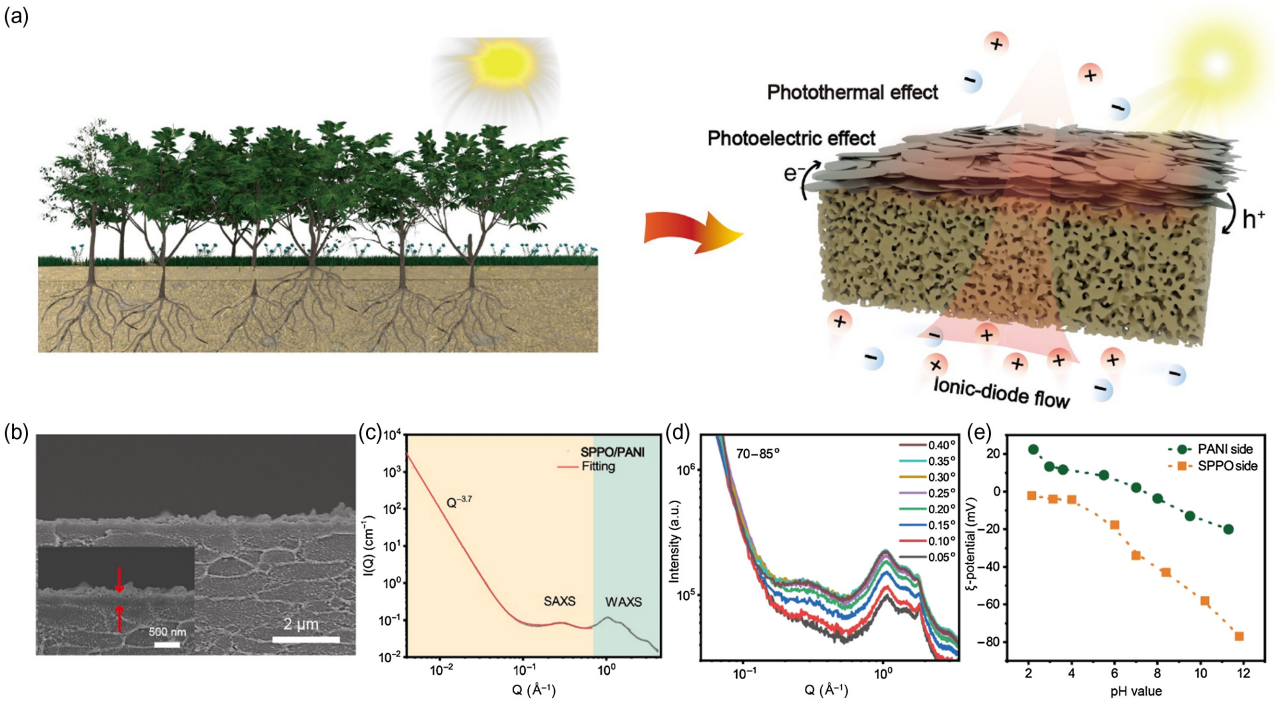

Figure 1 | *Preparation and characterization of SPPO/PANI heterogeneous membrane. (a) Schematic depiction of the heterogeneous membrane, inspired by plant growth and photosynthesis; (b) Cross-sectional SEM images of SPPO/PANI membrane; (c) SAXS/WAXS profile of SPPO/PANI membrane; (d) GISAXS/GIWAXS out plane (Structural information perpendicular to the film surface direction) profile of SPPO/PANI membrane on a silicon wafer; and (e) ζ-potential values of SPPO and PANI side.*

100 kHz field modulation with the amplitude set to 1G. The g-values for each EPR spectrum were extracted from simulations performed using EasySpin v5.2.23 (https://easyspin.org/). UV–vis spectrophotometer (Lambda 950, PerkinElmer, USA) was used to evaluate the membranes' absorption in the ultraviolet and visible light regions. The steady-state photoluminescence (PL) emission spectra were obtained at an excitation wavelength of 365 nm to evaluate the electron and hole separation performance by a fluorescence spectrometer (FLS1000, Edinburgh Instruments, Scotland, UK). The photothermal performance of SPPO and SPPO-PANI membranes was observed using an IR thermal imaging camera (FTIR ONE pro; USA). The ultraviolet photoelectron spectroscopy (UPS) measurement was performed on a Escalab 250 Xi spectrometer (Thermo Scientific, Massachusetts, USA) equipped with a monochromatic He I light source (21.22 eV). Small-angle/wide-angle X-ray scattering (SAXS/WAXS) experiments were conducted using a laboratory-based SAXS-WAXS beamline, KWS-X (XENOCS XUESS 3.0 XL, Grenoble, France). The membrane properties, including ion exchange capacity, water uptake and swelling ratio, and ion selectivity were determined, as well as the operation of the electrical measurements about ion-selective transport, osmotic power generation, and photoresponsive ion transport. The details are shown in the characterization section of the Supporting Information section "Characterization". The corresponding calculation section is also shown in part of Supporting Information section "Calculation". Several theoretical calculations about the mechanism of diode behavior and photothermal driven ion transport, potential distribution for PANI under light irradiation were performed, and density functional theory (DFT) theoretical calculation for electron migration within SPPO/PANI was also executed.

Results and Discussion

Structure design and characterization

Considering targeting as an efficient platform for osmotic-solar energy conversion, we proposed a multiscale heterogeneous SPPO/PANI membrane, drawing inspiration from natural plant growth and photosynthesis (Figure 1a). Having been motivated by seed sowing and plant growth, the involved electrostatic interactions (PPO~SO_3^-...^+H_3N~ANI) were utilized to facilitate ANI heteronucleation anchoring at the surface and extending several nanometers into the SPPO substrate (seeding), and then the PANI layer continued to grow outwards through polymerization (growing). The resultant SPPO/PANI heterostructure was readily stable, similar to the

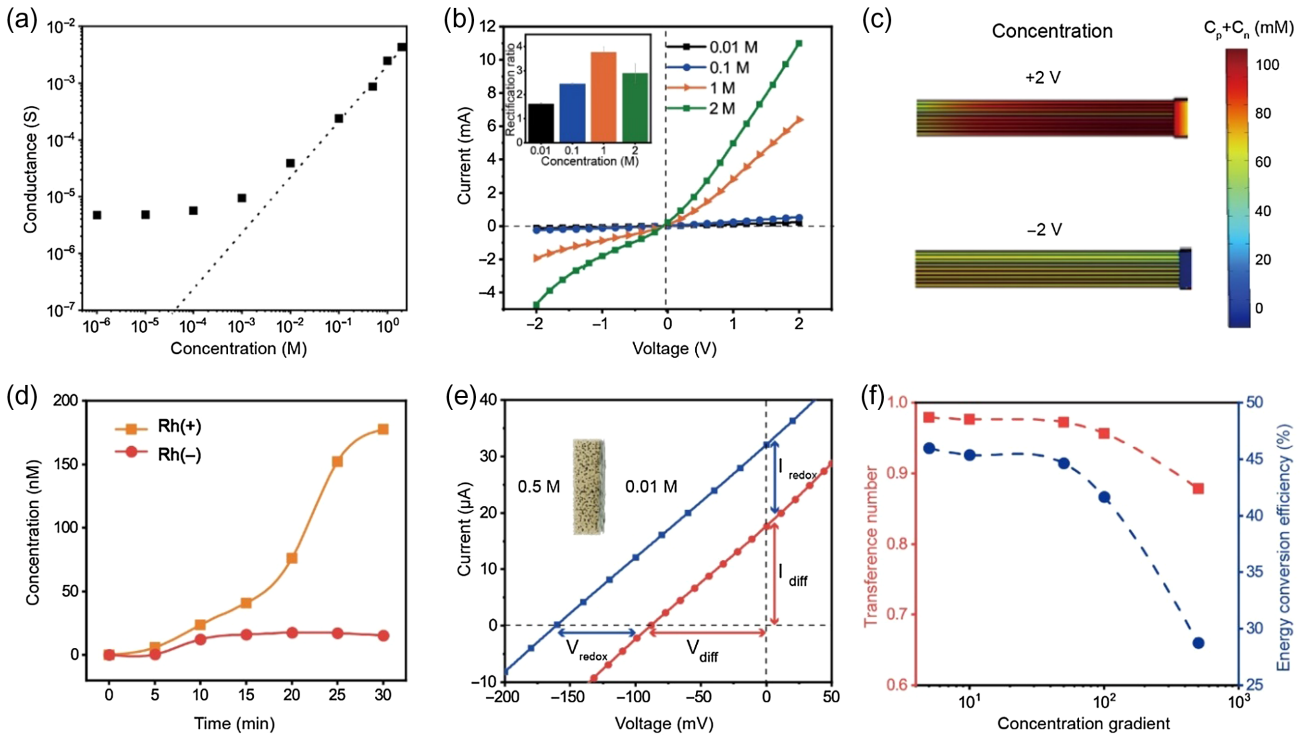

Figure 2 | *Transmembrane ion transport performance. (a) Ion conductance of SPPO/PANI membrane under different KCl concentrations; (b) I–V curves and the calculated rectification ratios (inset) of SPPO/PANI membrane in KCl solutions with different concentrations; (c) Numerical simulation for ionic concentration profile along X axial position at ±2 V; (d) Time-dependent concentration curves of the permeation test using two opposite charged dyes; (e) I–V curves of the membrane at 0.5 M/0.01 M gradient, with SPPO side facing high-concentration solution; and (f) Transference number and energy conversion efficiency under different concentration gradients.*

plant rooting in the land. The process of solar energy conversion in green plants, known as photosynthesis, involves the movement of protons or ions across cell membranes under light irradiation, creating an imbalanced distribution of charges that drives adenosine triphosphate (ATP) synthesis, the available cellular energy source. Similarly, under light irradiation, ion transport could be facilitated and the energy conversion output of the membrane would be enhanced based on the intrinsic photothermal and photoelectric properties of the PANI layer. Based on these, as the design principles, the SPPO/PANI membrane holds unique characteristics, as follows.

First, the heterostructure was equipped with multi-asymmetries, including structure geometry, pore size, and surface charge, enabling a diode-like behavior. PPO is a well-known inexpensive and thermally stable engineering plastic, whose sulfonation can be easily operated and controlled.[34,35] Thus, SPPO is a promising material for the selective matrix due to its merits, including reasonable cost, facile synthesis, good mechanical strength, and a remarkable membrane-forming property. Subsequently, a robust heterogeneous SPPO/PANI membrane was strategically constructed by in-situ polymerization of ANI monomers on top of the SPPO membrane. As shown in Figure 1b, a thin PANI layer with a thickness of ~280 nm is integrated with the SPPO matrix (~4.7 μm). Figure 1c shows the SAXS/WAXS profile of the SPPO/PANI membrane, suggesting a hierarchical structure of the SPPO matrix through three distinct scattering regions. Thereinto, the apparent middle range (0.01–0.06 $Å^{-1}$) a broad peak (with I_{max} ~ 0.25 $Å^{-1}$) was attributed to the nanophase separation within the amorphous portion of SPPO, where the average distance correlation length (ξ) was ~11 Å.[36] This correlation length represented the average distance between nanophases and corresponded to the mesh size of the dense membrane. Grazing-incidence small-angle X-ray scattering and grazing-incidence wide-angle X-ray scattering (GISAXS and GIWAXS) techniques were also employed. In Supporting Information Figure S1, the external PANI exhibited a nano sheet-like structure (sheet dimension exceeding 100 nm) distributed somewhat unevenly across the surface of the SPPO layer, and thus, characterized as a loose layer. The pore size of the PANI layer was estimated to be ~30 nm (Supporting Information Figure S3). By varying the incident angle slightly, structural information could be probed at different depths (Figure 1d and Supporting

Information Figure S2). As shown in Figure 1d, as the angle increased, a scattering peak (~1.83 $Å^{-1}$) ascribed to crystallized PANI diminished and shifted slightly towards smaller Q values, indicating that the incident depth extended into the region where PANI and SPPO made contact. This indicated the presence of a gradient heterostructure in SPPO/PANI. Moreover, the negatively charged SPPO and positively charged PANI layer exhibited a Janus-like surface potential of the membrane (Figure 1e). Additionally, the PANI layer was more hydrophilic than the SPPO layer (Supporting Information Figure S4).

Second, the comprehensive multiscale heterostructure contributed significantly to the sufficient transmembrane ionic transport, combining diode-like behavior and light-enhanced ion transport. The well-tailored SPPO matrix with interconnect three-dimensional (3D) nanochannels and high negative-charge density, played a primary role in the screening layer to ensure the permselectivity and transmembrane conductivity. Meanwhile, in addition to its role as an asymmetric element, the PANI layer could also serve as a light-responsive heterojunction for ion pumping due to the inherent photothermal effect and semiconductor photoelectric property.

Last but not least, the membrane possesses an enhanced anti-swelling capability (swelling ratio of ~1.69%), an excellent mechanical property (tensile strength of ~32.9 MPa), high interfacial stability (adhesion strength exceeding 430 J m^{-2}), and good thermal endurance (Supporting Information Figures S5 and S6).

Transmembrane ion transport

The obtained SPPO/PANI membrane was utilized as a separator in a double-chamber electrochemical cell to study ion transport properties. Herein, KCl was selected as the probe electrolyte owing to the similar ion diffusivities of K^+ and Cl^-.[12] As shown in Figure 2a, the conductance of the bulk KCl solution initially followed a proportional relationship with the concentration (dashed line). However, a deviation from this linear relationship appeared when the KCl concentration dropped below 0.1 M, indicating a surface-charge-governed ion transport behavior within the membrane. The Debye length (λ_D) was calculated to be 1 nm for 0.1 M KCl solutions, and $2\lambda_D$ exceeded the average size of the membrane (~1.1 nm), resulting in the overlap of electric double layers inside the ion channels.[37]

The representative phenomenon of ionic current rectification (ICR) was also evident in the current–voltage curves recorded at a symmetric voltage of ±2 V in KCl solutions of varying concentrations (Figure 2b). The current value under positive potential was higher than that of negative potential; thus, exhibited the preferential movement of cations (K^+) from SPPO to PANI, revealing a diode-like effect of the membrane. Remarkably, the ionic rectification was observed across a wide range of ionic concentrations, with the highest value found at 1 M of solution (ca. 3.76). Noteworthily, rectified ion fluxes were rarely observed in highly concentrated solutions (above 0.1 M) due to the shielding of surface charges on the channels.[38] Furthermore, the rectification ratios slightly varied with pH changes (Supporting Information Figure S7). The impressive ICR capability was ascribed to its multilevel asymmetric characteristics of the membrane, including surface charge, pore size, and geometry. This allowed the device to effectively capture osmotic energy from high-saline water resources. Especially, the homogeneous, highly negatively charged, and dense structure of SPPO, played a crucial role in this phenomenon. The ICR property of the SPPO/PANI membrane was further validated through a numerical calculation based on the Poisson–Nernst–Planck (PNP) equations (Supporting Information Figure S8). Within the SPPO/PANI hetero-channel, an ion enrichment region was formed under a positive bias (+2V), while an obvious ion depletion was observed when applied with a negative bias (−2V) (Figure 2c).

The membrane's ion selectivity was assessed by a permeation experiment using fluorescent dye molecules: Rhodamine 6G [Rh(+)] and sulforhodamine [Rh(−)]. As depicted in Figure 2d, our SPPO/PANI membrane exhibited a significantly higher permeate rate of Rh(+) than Rh(−), confirming the excellent cation selectivity of the designed membrane.

The transmembrane ionic transport properties were further examined via an asymmetric NaCl solution setup with a pair of homemade Ag/AgCl electrodes (Figure 2e). Using artificial seawater and river (0.5 M and 0.01 M NaCl), the open-circuit potential (V_{oc}) and short-circuit current (I_{sc}) were directly read as 161.2 mV and 31.5 μA, respectively. The generated open-circuit potential consisted of the osmotic potential (V_{diff}) and redox potential (V_{redox}), originating from the membrane and the unequal potential drop at the electrode–solution interface.[13] After subtracting the contribution of V_{redox} from the electrodes (Supporting Information Table S1), the membrane delivered a high net osmotic voltage of 88.2 mV and an osmotic current of 17.3 μA. The I–V curves were also measured in both forward and reverse diffusion directions (Supporting Information Figure S9). A preferential transport from SPPO to PANI side was evidenced by a lower internal membrane resistance calculated (5.09 vs 6.35 kΩ).

With a concentration gradient ranging from 5 to 500-fold, both the osmotic potential and current generally increased along with the rising concentration gradients. At a 500-fold concentration gradient, they reached high values of 120 mV and 35.5 μA, respectively, showing high ion diffusion flux and cation selectivity of the SPPO/PANI membrane (Supporting Information Figure S10). Furthermore, the cation transference numbers (t_+) and energy

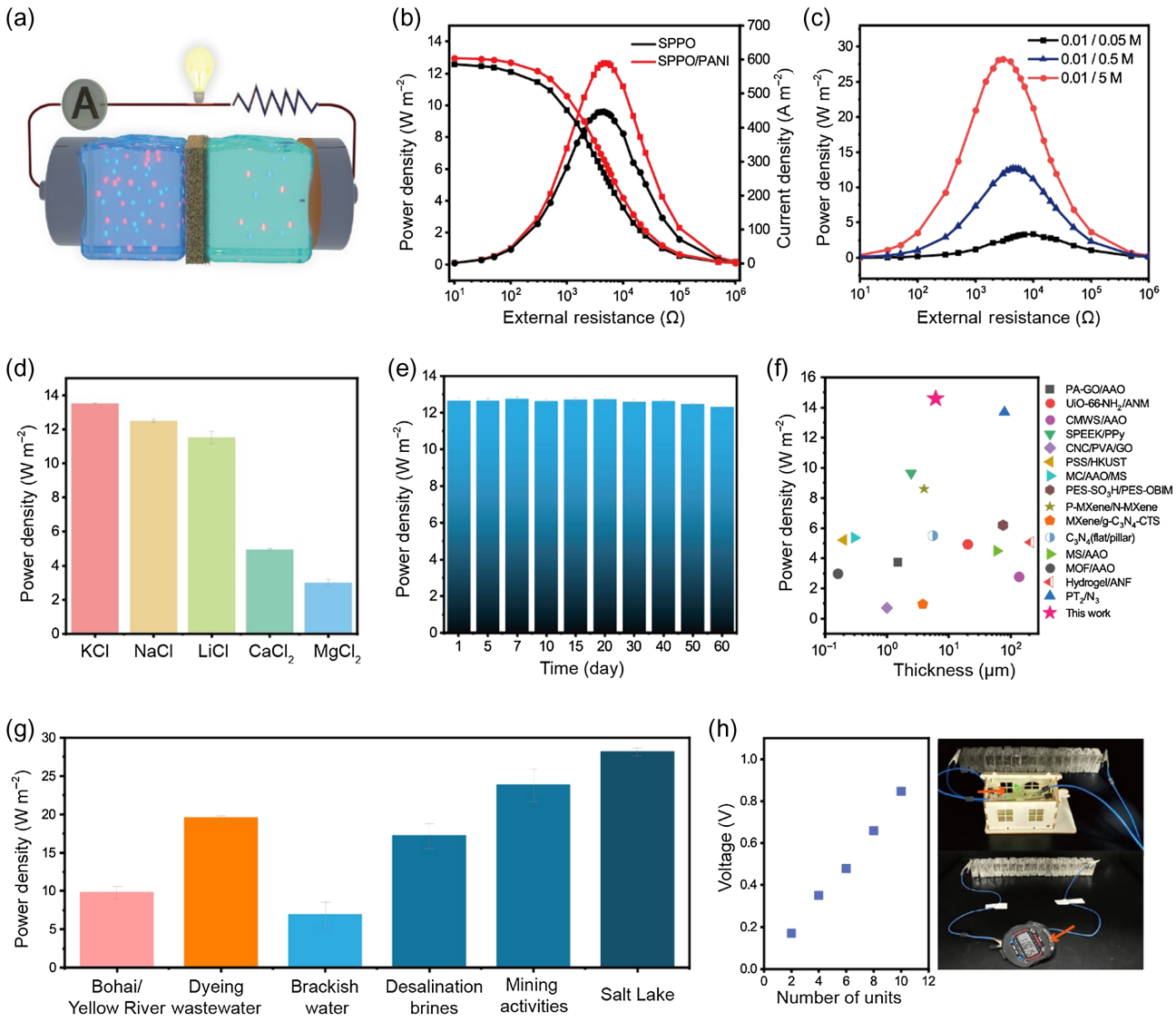

Figure 3 | *Output power density of SPPO/PANI membrane-based osmotic power generator. (a) Schematic of an osmotic energy conversion device under a concentration gradient; (b) Osmotic energy conversion of SPPO and SPPO/PANI membranes under a 50-fold concentration gradient (0.01 M/0.5 M NaCl); (c) Output osmotic power density of SPPO/PANI as a function of the increasing external resistance under 5, 50, and 500-fold NaCl salinity gradients. The low concentration was fixed at 0.01 M. (d) Peak power density with various electrolyte solutions; (e) Working stability of SPPO/PANI membrane; (f) Comparison of osmotic energy output with the state-of-the-art heterogeneous membranes; (g) Power generation of SPPO/PANI osmotic power generator with real and simulated water resources; (h) Units connected in series vs output voltage, and the tandem devices to power a calculator or LED light.*

conversion efficiency (η) of the SPPO/PANI membrane were calculated (Figure 2f). Under a 50-fold salinity gradient, the high t_+ value of 0.9725 was attributed to the adequate overlap of the electric double layers within the membrane-confined channel, corresponding to the outstanding cation selectivity. Thus, the energy conversion efficiency was favorably high, reaching up to 44.6%. This value ranked among the highest reported for membranes under similar conditions (Supporting Information Table S2).

Osmotic energy generation performance

The osmotic energy conversion capability of the SPPO/PANI membrane was investigated thoroughly. As shown in Figure 3a, the generated electric power could be extracted under a salinity gradient by supplying an external circuit with a load resistance. The output power density could be calculated using the equation $P = I^2R_L/S$, where I is the recorded current after calibration, R_L refers to the load resistance and S is the effective testing area. Figure 3b shows that the current density declined as the

load resistance increased. The maximum output power density occurred when the load resistance equaled the internal resistance of the membrane ($R_L = R_M$). At a 50-fold salinity gradient corresponding to artificial sea/river water (0.01/0.5 M NaCl), the SPPO/PANI membrane achieved a prominent maximum osmotic power density of 12.6 W m^{-2} with an external resistance of 4.5 KΩ. The ultralow resistance was attributed to short and effective ionic transport channels throughout the membrane.

The significantly enhanced performance of the SPPO/PANI membrane compared with the pristine SPPO membrane could be primarily attributed to the thoughtful design of its asymmetrical structure.[5] For low R_L, $P \approx I^2R_L/S$, where the generated current mainly flowed and dissipated through the load resistance. Under this condition, there was no obvious difference between the pristine SPPO and SPPO/PANI. For high R_L, $P \approx I^2R_M/S$, the generated current mainly circulated in a loop within the membrane, leading to more osmotic power loss within the membrane. Nevertheless, in the case of the SPPO/PANI membrane, with oppositely charged dual layers, the negatively charged SPPO matrix was positioned to face the highly concentrated solution, serving as the selective layer, which allowed cations (counterions) to pass and repel anions. Meanwhile, the positively-charged PANI layer facing the low concentration side could prevent the accumulation of counterions (cations), eliminating polarization, thereby enhancing the energy conversion efficiency. Additionally, the ionic diode-like behavior of the heterogeneous membrane could promote unidirectional ion transport and reduce the dissipation of Gibbs free energy as Joule heating reversed by hindering the ion flow back.[1,4,38]

The influence of PANI growth on the membrane morphology and power density was also meticulously investigated (Supporting Information Figures S11 and S12). The thickness of the PANI layer was modulated by varying the cycle number of the in-situ polymerization process. These results suggested that a single polymerization cycle was insufficient to form a complete functional layer with optimal performance. Conversely, excessive PANI growth increased the membrane thickness and transport resistance, both of which were detrimental to energy harvesting. Therefore, the optimized energy conversion ability of the SPPO/PANI membrane was achieved through a carefully controlled polymerization process.

The energy conversion performance of the SPPO/PANI membrane was further accessed under various salinity gradients, electrolytes, and pH conditions. As shown in Figure 3c, the output osmotic power density increased significantly from 3.34 to 28.2 W m^{-2}, as the salinity gradient increased from 5 to 500-fold, illustrating the great potential of the SPPO/PANI membrane for collecting osmotic energy in high salinity environments. Figure 3d revealed that the membrane's power output was markedly influenced by the type of electrolytes used. Cations with a larger diffusion coefficient contributed to a higher current, reaching a maximum power output of 13.5 W m^{-2} for KCl, with the largest diffusion coefficient of K^+ ions.[28] Additionally, the membrane was capable of working efficiently and steadily across a wide pH range (Supporting Information Figure S13). Notably, after a testing period of 60 days, the output osmotic power density remained virtually unchanged, as a result of stable membrane structure (Figure 3e and Supporting Information Figure S14), demonstrating the outstanding long-term working endurance of the membrane. The exceptional adaptability and stability made the SPPO/PANI membrane a promising candidate for practical applications in high-performance energy-harvesting devices.

To vividly highlight the advantages of the SPPO/PANI membrane, Figure 3f displays the comparison of its performance with the state-of-the-art heterogeneous bilayer membranes in terms of thickness and net osmotic energy output density.[8,9,13,28,31,32,39−47] Apparently, the SPPO/PANI membrane exhibited a distinct superior output power density. Furthermore, the excellent robustness and scalability of the membrane allowed for easy customization of its area to generate the desired power output. Across a range of testing areas (0.03–28.26 mm^2), the SPPO/PANI membrane consistently delivered an advantageous power density, outperforming most recently reported membranes (Supporting Information Figure S15).[6,7,13,28,37,42−44,48−52]

The membrane's performance was also remarkable when applied to different salty sources. By applying natural seawater (from China Bohai) and river water (from China Yellow River), a net power density output of 9.82 W m^{-2} was recorded, far surpassing the commercial benchmark of 5 W m^{-2} (Figure 3g).

The textile industry generates a vast amount of wastewater containing residual dyes and inorganic salts during dyeing and finishing processes. Despite this resource's potential, there is rare research on harnessing osmotic energy from textile wastewater. Thus, we explored the electrical energy extraction capability of primary textile wastewater using the SPPO/PANI membrane-based energy generator. By mixing real dyeing residual wastewater and river water, impressively, the membrane achieved a high and durable osmotic output power density of 19.6 W m^{-2}, highlighting its potential for extracting energy from complex industrial wastewater (Figure 3g and Supporting Information Figure S16). The membrane also demonstrated versatility and adaptability when tested with various simulated wastewaters and brines, yielding osmotic power densities of 6.92, 17.2, 23.8, and 28.1 W m^{-2} for brackish water, desalination brines, mining wastewater, and Salt Lake water, respectively.

To showcase its practical application, a scaled-up membrane-based generator was constructed using the

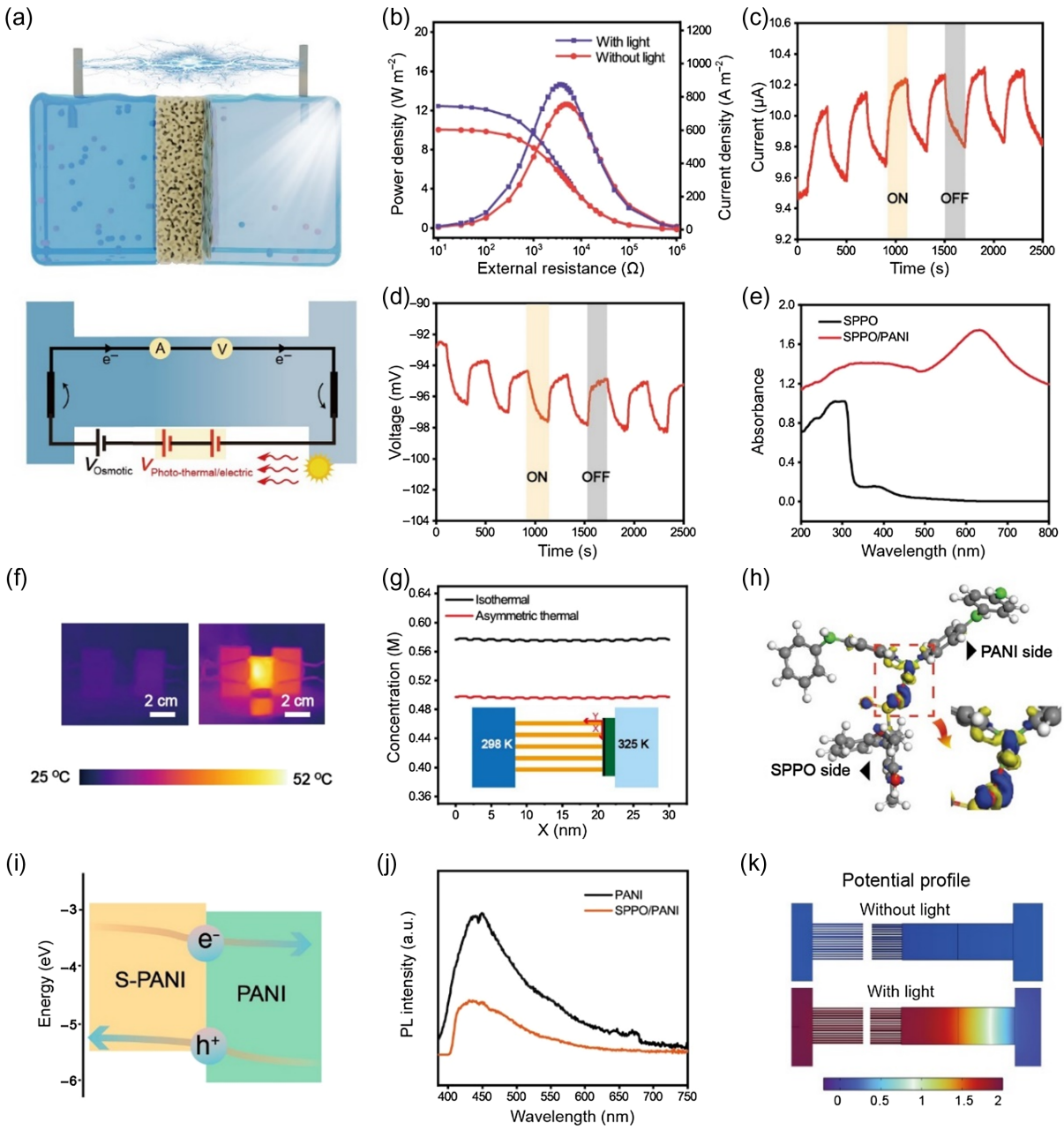

Figure 4 | *Light-enhanced osmotic energy conversion behavior. (a) Schematic of the osmotic-solar power generator and the equivalent circuit; (b) Power generation of SPPO/PANI membrane without/with light irradiation; (c) Current-time curve recorded without/with light; (d) Potential-time curve obtained without/with light; (e) UV–vis spectra of SPPO and SPPO/PANI membranes; (f) IR thermal images of the SPPO/PANI membrane without/with light illumination; (g) Simulation for ion enrichment effect in low concentration side under isothermal and asymmetric photothermal conditions; (h) Charge density difference of the interfacial SPPO/PANI; (i) Schematic of interfacial band alignment and photoinduced charge carriers' transfer; (j) PL spectra of PANI and SPPO/PANI membranes; and (k) Potential distribution in SPPO/PANI without/with light irradiation.*

SPPO/PANI membrane (Figure 3h). The output voltage increased linearly along with the number of units in the stack. A 17-unit stack could readily power a stopwatch or light up a green light-emitting diode (LED) light, suggesting the blooming potential of the SPPO/PANI membrane for blue energy harvesting applications.

Light-enhanced ion transport and energy output

Analogous to plant photosynthesis, the energy output of our system can be further enhanced by absorbing light and boosting ion transport (Figure 4a). As shown in Figure 4b, under light irradiation (100 mW cm^{-2}), the

output power density increased to 14.6 W m^{-2} for a 0.01/0.5 M NaCl gradient system. When the light was switched on, there was a stable and consistent increase in both current and voltage, which sharply decreased once the light was turned off (Figure 4c,d). Additionally, light inspired a net ionic current and voltage even in a symmetrical solution system (0.01 M KCl), indicating a light-enhanced ion transport and energy output behavior (Supporting Information Figure S17). The stirring light-boosting performance of the SPPO/PANI membrane was attributed to the rational design of its heterogeneous structure and composition. Primarily, the intrinsic photothermal and photoelectric properties of the PANI layer played a crucial role in the enhancement.

From the UV–vis adsorption spectrum (Figure 4e), SPPO/PANI showed a significantly broader adsorption range of 300–700 nm, indicating a strong absorption capability for both UV and visible light. As recorded by an IR thermal camera (Figure 4f), the temperature on the PANI side of the membrane rapidly increased to ~52 °C within seconds of light exposure. Such high-efficiency light-to-heat conversion could forthwith establish a temperature gradient across the membrane, driving ion migration from the cold (SPPO) side to the hot (PANI) side.[27] This phenomenon was supported by theoretical simulation based on the PNP theory, as illustrated in Figure 4g. The simulation predicted a lower ion concentration enrichment found near the boundary between the SPPO and the PANI layer under an asymmetric thermal condition.[53] The preferential migration of ions from the SPPO to the PANI side was advantageous for the system. By positioning the PANI side facing the low-concentration side and exposing it to light, a synergy was achieved between the imposed salinity gradient and the light-induced temperature gradient. The photothermally evaluated temperature on the PANI side, that is, the low concentration side, helped to mitigate the ion concentration polarization effect and improved the confined ion transport.[53,54]

The presence of PANI in the SPPO/PANI membrane offered unique advantages due to its properties as a polymer semiconductor. When exposed to light, PANI could be excited, leading to the generation of excitons.[55] From the EPR spectra (Supporting Information Figure S18), the presence of free electrons and the corresponding vacancies were confirmed by a single and narrow signal with a g-value of ~2.004.[56] Upon light illumination, these excitons tended to separate and diffuse, leading to an asymmetric charge distribution.[57] Nevertheless, the capacity for charge separation remained highly constrained due to insufficient exciton diffusion and rapid electron-hole recombination.[27]

In the case of the SPPO/PANI membrane, a delicate heterojunction was built to promote the dissociation of excitons and the transfer of charge carriers, by patterning two types of PANI with different band structures. During the PANI growing process, the amine groups from ANI monomers would accept protons from the sulfonic acid groups of SPPO, forming sulfonic acid doped PANI (PPO~SO_3^-...$^+$HN.~PANI, denoted as S-PANI) rooting at the surface and extending several nanometers into the SPPO substrate (Supporting Information Figure S19). The PANI layer continued to grow outwards with the addition of HCl as a doping reagent, resulting in vertically stacked repeating units and tiled sheet-like structures. Both the strongly connected interface and the special geometry of the PANI layer were propitious to the transmission of photoinduced charge carriers.

To verify the formation of PANI heterojunction consisting of S-PANI and external PANI, the electronic structure of the interfacial S-PANI was initially calculated using DFT (Figure 4h and Supporting Information Figures S20 and S21). As shown in Figure 4h, the yellow (blue) parts represent the regions of electron accumulation (depletion), displaying a possible electron transfer within S-PANI. Furthermore, to investigate the transport mechanism for S-PANI and external PANI heterojunction, the interfacial band alignment was derived using ultraviolet photoelectron spectra and UV–vis absorption spectra.[16,58] Based on the determination (Supporting Information Figures S22 and S23), the highest occupied molecular orbital (HOMO) and lowest unoccupied molecular orbital (LUMO) levels of S-PANI were higher than those of PANI within the overlap range of the bandgaps. As shown in Figure 4i, this arrangement facilitated the migration of photo-induced electrons and holes.[59] Therefore, the separation of photoinduced carriers was improved within the heterogeneous SPPO/PANI membrane, as evidenced by its significantly weaker PL intensity compared with pure PANI (Figure 4j). Under light illumination, the photogenerated holes accumulated on the S-PANI (left) side of the interface, while electrons accumulated on the PANI (right) side. This was confirmed through COMSOL Multiphysics calculation and analysis (Supporting Information Figures S24 and S25). Then the resulting photo-enhanced potential distribution was confirmed, as shown in Figure 4k. Within SPPO/PANI heterochannels, the observed intensive potential distribution under light irradiation provided evidence for the formation of light-enhanced transmembrane potential.

Collectively, the sophisticated heterostructure and synergistic photothermal/electric effect of the SPPO/PANI membrane contributed to its exceptional performance in osmotic and solar energy harvesting. This unique design enhanced cation selectivity and permeability, ultimately facilitating efficient light-driven ion transport and boosting the overall energy output.

Conclusion

We successfully developed a bioinspired multiscale heterogeneous (SPPO/PANI) membrane as a promising

platform for harvesting both osmotic and solar energy, facilely fabricated through in-situ polymerization of ANI monomers on top of an SPPO matrix. The robust and compatible heterostructure of the SPPO/PANI granted high ion conductivity and selectivity. The multilevel asymmetric architecture encompassing surface charge, pore geometry, and chemical composition, enabled the SPPO/PANI membrane with diode-like behavior, facilitating unidirectional ion diffusion and suppressing the dissipation of Gibbs free energy. Consequently, a superior osmotic power conversion was achieved in various water sources with different gradients. For example, an ultrahigh osmotic output power density of up to 12.6 W m^{-2} could be produced by applying artificial seawater and river water. An impressive net output power density of 19.6 W m^{-2} could be harvested by mixing real dyeing residual wastewater and river water. Notably, with light irradiation, the output power density of the SPPO/PANI membrane could be further elevated. The experimental and theoretical simulation results suggested that the PANI layer's efficient light-to-heat conversion created a temperature gradient within the membrane. Additionally, the intricate PANI heterojunction facilitated the transfer and separation of photoinduced carriers, leading to the generation of a transmembrane potential. Thus, an active ion transport through the membrane could be triggered directionally through the synergic photothermal and photoelectric effect, enabling the conversion of osmotic and solar energy. This work is dedicated to designing and manufacturing advanced membrane-based power generators, capable of harnessing sustainable resources such as osmotic and solar energy.

Supporting Information

Supporting Information is available, and includes a characterization section, calculation section, supplementary figures, and supplementary tables.

Conflict of Interest

There is no conflict of interest to report.

Funding Information

The authors gratefully acknowledge the financial support of the National Natural Science Foundation of China (NSFC; grant no. 21991123). We are also very grateful for the kind support from the National Innovation Center of Advanced Dyeing and Finishing Technology, Shandong, China.

Acknowledgments

The authors appreciate Prof. Zheng Tang from Donghua University, China, for his helpful discussion regarding the PANI heterojunction.

References

1. Siria, A.; Bocquet, M. L.; Bocquet, L. New Avenues for the Large-Scale Harvesting of Blue Energy. *Nat. Rev. Chem.* **2017**, *1*, 0091.
2. Macha, M.; Marion, S.; Nandigana, V. V. R.; Radenovic, A. 2D Materials as an Emerging Platform for Nanopore-Based Power Generation. *Nat. Rev. Mater.* **2019**, *4*, 588–605.
3. Xin, W.; Jiang, L.; Wen, L. Two-Dimensional Nanofluidic Membranes Toward Harvesting Salinity Gradient Power. *ACC. Chem. Res.* **2021**, *54*, 4154–4165.
4. Chen, W.; Xiang, Y.; Kong, X.-Y.; Wen, L. Polymer-Based Membranes for Promoting Osmotic Energy Conversion. *Giant* **2022**, *10*, 100094.
5. Huang, X.; Kong, X.-Y.; Wen, L.; Jiang, L. Bioinspired Ionic Diodes: From Unipolar to Bipolar. *Adv. Funct. Mater.* **2018**, *28*, 1801079.
6. Li, C.; Wen, L.; Sui, X.; Cheng, Y.; Gao, L.; Jiang, L. Large-Scale, Robust Mushroom-Shaped Nanochannel Array Membrane for Ultrahigh Osmotic Energy Conversion. *Sci. Adv.* **2021**, *7*, eabg2183.
7. Bian, G.; Pan, N.; Luan, Z.; Sui, X.; Fan, W.; Xia, Y.; Sui, K.; Jiang, L. Anti-Swelling Gradient Polyelectrolyte Hydrogel Membranes as High-Performance Osmotic Energy Generators. *Angew. Chem. Int. Ed.* **2021**, *133*, 20294–20300.
8. Sun, Y.; Dong, T.; Lu, C.; Xin, W.; Yang, L.; Liu, P.; Qian, Y.; Zhao, Y.; Kong, X. Y.; Wen, L.; Jiang, L. Tailoring A Poly(ether Sulfone) Bipolar Membrane: Osmotic-Energy Generator with High Power Density. *Angew. Chem. Int. Ed.* **2020**, *59*, 17423–17428.
9. Ding, L.; Zheng, M.; Xiao, D.; Zhao, Z.; Xue, J.; Zhang, S.; Caro, J.; Wang, H. Bioinspired $Ti_3C_2T_x$ MXene-Based Ionic Diode Membrane for High-Efficient Osmotic Energy Conversion. *Angew. Chem. Int. Ed.* **2022**, *61*, e202206152.
10. Zhang, X.; Wen, Q.; Wang, L.; Ding, L.; Yang, J.; Ji, D.; Zhang, Y.; Jiang, L.; Guo, W. Asymmetric Electrokinetic Proton Transport Through 2D Nanofluidic Heterojunctions. *ACS Nano* **2019**, *13*, 4238–4245.
11. Tonnah, R. K.; Chai, M.; Abdollahzadeh, M.; Xiao, H.; Mohammad, M.; Hosseini, E.; Zakertabrizi, M.; Jarrahbashi, D.; Asadi, A.; Razmjou, A.; Asadnia, M. Bioinspired Angstrom-Scale Heterogeneous MOF-on-MOF Membrane for Osmotic Energy Harvesting. *ACS Nano* **2023**, *17*, 12445–12457.
12. Cao, L.; Chen, I.-C.; Chen, C.; Shinde, D. B.; Liu, X.; Li, Z.; Zhou, Z.; Zhang, Y.; Han, Y.; Lai, Z. Giant Osmotic Energy Conversion through Vertical-Aligned Ion-Permselective Nanochannels in Covalent Organic Framework Membranes. *J. Am. Chem. Soc.* **2022**, *144*, 12400.
13. Pan, S.; Liu, P.; Li, Q.; Zhu, B.; Liu, X.; Lao, J.; Gao, J.; Jiang, L. Toward Scalable Nanofluidic Osmotic Power

Generation from Hypersaline Water Sources with a Metal–Organic Framework Membrane. *Angew. Chem. Int. Ed.* **2023**, *62*, e202218129.
14. Lu, J.; Jiang, Y.; Xiong, T.; Yu, P.; Jiang, W.; Mao, L. Light-Regulated Nanofluidic Ionic Diodes with Heterogeneous Channels Stemming from Asymmetric Growth of Metal-Organic Frameworks. *Anal. Chem.* **2022**, *94*, 4328–4334.
15. Hu, Y.; Teng, Y.; Sun, Y.; Liu, P.; Fu, L.; Yang, L.; Kong, X.-Y.; Zhao, Q.; Jiang, L.; Wen, L. Bioinspired Poly (ionic Liquid) Membrane for Efficient Salinity Gradient Energy Harvesting: Electrostatic Crosslinking Induced Hierarchical Nanoporous Network. *Nano Energy* **2022**, *97*, 107170.
16. Yang, J.; Liu, P.; He, X.; Hou, J.; Feng, Y.; Huang, Z.; Yu, L.; Li, L.; Tang, Z. Photodriven Active Ion Transport Through a Janus Microporous Membrane. *Angew. Chem. Int. Ed.* **2020**, *132*, 6303–6307.
17. Wang, L.; Wen, Q.; Jia, P.; Jia, M.; Lu, D.; Sun, X.; Jiang, L.; Guo, W. Light-Driven Active Proton Transport Through Photoacid- and Photobase-Doped Janus Graphene Oxide Membranes. *Adv. Mater.* **2019**, *31*, 1903029.
18. Zhou, X.; Hu, X.; Yu, J.; Liu, S.; Shu, Z.; Zhang, Q.; Li, H.; Ma, Y.; Xu, H.; Zhai, T. 2D Layered Material-Based van der Waals Heterostructures for Optoelectronics. *Adv. Funct. Mater.* **2018**, *28*, 1706587.
19. Jia, P.; Wang, L.; Zhang, Y.; Yang, Y.; Jin, X.; Zhou, M.; Quan, D.; Jia, M.; Cao, L.; Long, R.; Jiang, L.; Guo, W. Harnessing Ionic Power from Equilibrium Electrolyte Solution via Photoinduced Active Ion Transport Through van-der-Waals-Like Heterostructures. *Adv. Mater.* **2021**, *33*, 2007529.
20. Jiang, Y.; Ma, W.; Qiao, Y.; Xue, Y.; Lu, J.; Gao, J.; Liu, N.; Wu, F.; Yu, P.; Jiang, L.; Mao, L. Metal–Organic Framework Membrane Nanopores as Biomimetic Photoresponsive Ion Channels and Photodriven Ion Pumps. *Angew. Chem. Int. Ed.* **2020**, *59*, 12795.
21. Zuo, X.; Zhu, C.; Xian, W.; Meng, Q. W.; Guo, Q.; Zhu, X.; Wang, S.; Wang, Y.; Ma, S.; Sun, Q. Thermo-Osmotic Energy Conversion Enabled by Covalent-Organic-Framework Membranes with Record Output Power Density. *Angew. Chem. Int. Ed.* **2022**, *61*, e202116910.
22. Zhou, Y.; Jiang, L. Bioinspired Nanoporous Membrane for Salinity Gradient Energy Harvesting. *Joule* **2020**, *4*, 2244–2248.
23. Liu, P.; Zhou, T.; Yang, L.; Zhu, C.; Teng, Y.; Kong, X.-Y.; Wen, L. Synergy of Light and Acid–Base Reaction in Energy Conversion based on Cellulose Nanofiber Intercalated Titanium Carbide Composite Nanofluidics. *Energy Environ. Sci.* **2021**, *14*, 4400.
24. Lee, K. H.; Zhang, Y.-Z.; Jiang, Q.; Kim, H.; Alkenawi, A. A.; Alshareef, H. N. Ultrasound-Driven Two-Dimensional $Ti_3C_2T_x$ MXene Hydrogel Generator. *ACS Nano* **2020**, *14*, 3199–3207.
25. Xin, W.; Jiang, L.; Wen, L. Engineering Bioinspired Self-Assembled Nanochannels for Smart Ion Transport. *Angew. Chem. Int. Ed.* **2022**, *61*, e202207369.
26. Liu, P.; Kong, X.-Y.; Jiang, L.; Wen, L. Ion Transport in Nanofluidics under External Fields. *Chem. Soc. Rev.* **2024**, *53*, 2972–3001.
27. Xiao, K.; Schmidt, O. G. Light-Driven Ion Transport in Nanofluidic Devices: Photochemical, Photoelectric, and Photothermal Effects. *CCS Chem.* **2022**, *4*, 54–65.
28. Wang, J.; Wang, D.; Song, Z.; Jiang, N.; Li, S.; Zhang, Y.; Huang, B.; Cui, Z.; Zhou, H.; Wang, L. Efficient Solar Energy Conversion via Bionic Sunlight-Driven Ion Transport Boosted by Synergistic Photo-Electric/Thermal Effects. *Energy Environ. Sci.* **2023**, *16*, 3146.
29. Wang, Q.; Wu, Y.; Zhu, C.; Hu, Y.; Fu, L.; Qian, Y.; Li, T.; Li, X.; Zhang, Z.; Kong, X.-Y.; Jiang, L.; Zhang, Z.; Wen, L. Efficient Solar-Osmotic Power Generation from Bioinspired Anti-Fouling 2D WS_2 Composite Membranes. *Angew. Chem. Int. Ed.* **2023**, *62*, e202302938.
30. Zhou, S.; Zhang, X.; Xie, L.; He, Y.; Yan, M.; Liu, T.; Zeng, H.; Jiang, L.; Kong, B. Dual-Functional Super-Assembled Mesoporous Carbon-Titania/AAO Hetero-Channels for Bidirectionally Photo-Regulated Ion Transport. *Small* **2023**, *19*, 2301038.
31. Zhang, L.; Pan, S.; Liu, Y.; Yu, L.; Huang, T.; Xia, J.; Liu, X.; Gao, J.; Sui, K.; Jiang, L. Janus Carbon Nitride Membrane for Robust and Enhanced Nanofluidic Power Generation from Wastewater. *Water Res.* **2023**, *242*, 120285.
32. He, Y.; Zhang, L.; Guo, L.; Geng, Y.; Ren, Y.; Liu, Y.; Fan, X.; Liu, W.; Zhai, J.; Wang, P.; Jiang, L. Bulk Heterojunction-Induced Ion Transport in Nanochannel Arrays for Light-Enhanced Osmotic Energy Conversion. *J. Mater. Chem. A* **2022**, *10*, 23823.
33. Kosmala, B.; Schauer, J. Ion-Exchange Membranes Prepared by Blending Sulfonated Poly(2,6-dimethyl-1,4-phenylene oxide) with Polybenzimidazole. *J. Appl. Polym. Sci.* **2002**, *85*, 1118–1127.
34. Xu, T.; Wu, D.; Wu, L. Poly(2,6-dimethyl-1,4-phenylene oxide) (PPO)—A Versatile Starting Polymer for Proton Conductive Membranes (PCMs). *Prog. Polym. Sci.* **2008**, *33*, 894–915.
35. Li, Y.; Liu, Y.; Xu, Z.; Yang, Z. Poly(phenylene Oxide)-Based Ion-Exchange Membranes for Aqueous Organic Redox Flow Battery. *Ind. Eng. Chem. Res.* **2019**, *58*, 10707–10712.
36. Schubert, K. V.; Strey, R.; Kline, S. R.; Kaler, E. W. Small Angle Neutron Scattering Near Lifshitz Lines: Transition from Weakly Structured Mixtures to Microemulsions. *J. Chem. Phys.* **1994**, *101*, 5343–5355.
37. Zhu, Q.; Li, Y.; Qian, Q.; Zuo, P.; Guiver, M. D.; Yang, Z.; Xu, T. A Sulfonated Ultramicroporous Membrane with Selective Ion Transport Enables Osmotic Energy Extraction from Multiform Salt Solutions with Exceptional Efficiency. *Energy Environ. Sci.* **2022**, *15*, 4148.
38. Zhu, X.; Hao, J.; Bao, B.; Zhou,Y.; Zhang, H.; Pang, J.; Jiang, Z.; Jiang, L. Unique Ion Rectification in Hypersaline Environment. *Sci. Adv.* **2018**, *4*, eaau1665.
39. Zhou, S.; Xie, L.; Zhang, L.; Wen, L.; Tang, J.; Zeng, J.; Liu, T.; Peng, D.; Yan, M.; Qiu, B.; Liang, Q.; Liang, K.; Jiang, L.; Kong, B. Interfacial Super-Assembly of Ordered Mesoporous Silica-Alumina Heterostructure Membranes with pH-Sensitive Properties for Osmotic Energy Harvesting. *ACS Appl. Mater. Interfaces* **2021**, *13*, 8782–8793.

40. Liu, Y.-C.; Yeh, L.-H.; Zheng, M.-J.; Wu, K. C.-W. Highly Selective and High-Performance Osmotic Power Generators in Subnanochannel Membranes Enabled by Metal-Organic Frameworks. *Sci. Adv.* **2021**, *7*, eabe9924.
41. Xie, L.; Zhou, S.; Liu, J.; Qiu, B.; Liu, T.; Liang, Q.; Zheng, X.; Li, B.; Zeng, J.; Yan, M.; He, Y.; Zhang, X.; Zeng, H.; Ma, D.; Chen, P.; Liang, K.; Jiang, L.; Wang, Y.; Zhao, D.; Kong, B. Sequential Superassembly of Nanofiber Arrays to Carbonaceous Ordered Mesoporous Nanowires and Their Heterostructure Membranes for Osmotic Energy Conversion. *J. Am. Chem. Soc.* **2021**, *143*, 6922–6932.
42. Hao, J.; Bao, B.; Zhou, J.; Cui, Y.; Chen, X.; Zhou, J.; Zhou, Y.; Jiang, L. A Euryhaline-Fish-Inspired Salinity Self-Adaptive Nanofluidic Diode Leads to High-Performance Blue Energy Harvesters. *Adv. Mater.* **2022**, *34*, 2203109.
43. Bang, K. R.; Kwon, C.; Lee, H.; Kim, S.; Cho, E. S. Horizontally Asymmetric Nanochannels of Graphene Oxide Membranes for Efficient Osmotic Energy Harvesting. *ACS Nano* **2023**, *17*, 10000–10009.
44. Zhang, X.; Li, M.; Zhang, F.; Li, Q.; Xiao, J.; Lin, Q.; Qing, G. Robust Cellulose Nanocrystal-Based Self-Assembled Composite Membranes Doped with Polyvinyl Alcohol and Graphene Oxide for Osmotic Energy Harvesting. *Small* **2023**, *19*, 2304603.
45. Zhou, S.; Xie, L.; Zhang, X.; Yan, M.; Zeng, H.; Liang, K.; Jiang, L.; Kong, B. Super-Assembled Multi-Level Asymmetric Mesochannels for Coupled Accelerated Dual-Ion Selective Transport. *Adv. Mater.* **2022**, *35*, 2208903.
46. Zhang, Z.; He, L.; Zhu, C.; Qian, Y.; Wen, L.; Jiang, L. Improved Osmotic Energy Conversion in Heterogeneous Membrane Boosted by Three-Dimensional Hydrogel Interface. *Nat. Commun.* **2020**, *11*, 875.
47. Xiao, J.; Cong, M.; Li, M.; Zhang, X.; Zhang, Y.; Zhao, X.; Lu, W.; Guo, Z.; Liang, X.; Qing, G. Self-Assembled Nanoporous Metal-Organic Framework Monolayer Film for Osmotic Energy Harvesting. *Adv. Funct. Mater.* **2023**, *34*, 2307996.
48. Safaei, J.; Gao, Y.; Hosseinpour, M.; Zhang, X.; Sun, Y.; Tang, X.; Zhang, Z.; Wang, S.; Guo, X.; Wang, Y.; Chen, Z.; Zhou, D.; Kang, F.; Jiang, L.; Wang, G. Vacancy Engineering for High-Efficiency Nanofluidic Osmotic Energy Generation. *J. Am. Chem. Soc.* **2023**, *145*, 2669–2678.
49. Yu, C.; Zhu, X.; Wang, C.; Zhou, Y.; Jia, X.; Jiang, L.; Liu, X.; Wallace, G. G. A Smart Cyto-Compatible Asymmetric Polypyrrole Membrane for Salinity Power Generation. *Nano Energy* **2018**, *53*, 475–482.
50. Man, Z.; Safaei, J.; Zhang, Z.; Wang, Y.; Zhou, D.; Li, P.; Zhang, X.; Jiang, L.; Wang, G. Serosa-Mimetic Nanoarchitecture Membranes for Highly Efficient Osmotic Energy Generation. *J. Am. Chem. Soc.* **2021**, *143*, 16206–16216.
51. Chen, C.; Liu, D.; He, L.; Qin, S.; Wang, J.; Razal, J. M.; Kotov, N. A.; Lei, W. Bio-Inspired Nanocomposite Membranes for Osmotic Energy Harvesting. *Joule* **2020**, *4*, 247–261.
52. Chen, L.; Qian, L.; Valentino, K. Y.; Dan, H.; Yusuke, Y.; Yiyong, M. Self-Assembly of Block Copolymers Towards Mesoporous Materials for Energy Storage and Conversion Systems. *Chem. Soc. Rev.* **2020**, *49*, 4681–4736.
53. Mai, V.-P.; Yang, R.-J. Boosting Power Generation from Salinity Gradient on High-Density Nanoporous Membrane Using Thermal Effect. *Appl. Energy* **2020**, *274*, 115294.
54. Wu, Y.; Xin, W.; Kong, X.-Y.; Chen, J.; Qian, Y.; Sun, Y.; Zhao, X.; Chen, W.; Jiang, L.; Wen, L. Enhanced Ion Transport by Graphene Oxide/Cellulose Nanofibers Assembled Membranes for High-Performance Osmotic Energy Harvesting. *Mater. Horiz.* **2020**, *7*, 2702.
55. Bhadra, S.; Khastgir, D.; Singha, N. K.; Lee, J. H. Progress in Preparation, Processing and Applications of Polyaniline. *Prog. Polym. Sci.* **2009**, *34*, 783–810.
56. Wu, K. H.; Lai, Y. S.; Shih, C. C.; Wang, G. P.; Yang, C. C. An EPR Investigation of Conductive Polyaniline–Poly(methyl Methacrylate-Co-Acrylic Acid) Blends. *Polym. Compos.* **2008**, *29*, 902–905.
57. Xiao, K.; Chen, L.; Chen, R.; Heil, T.; Lemus, S. D. C.; Fan, F.; Wen, L.; Jiang, L.; Antonietti, M. Artificial Light-Driven Ion Pump for Photoelectric Energy Conversion. *Nat. Commun.* **2019**, *10*, 74.
58. Li, L.; Luo, C.; Chen, X.; Chu, N.; Li, L.; Chao, M.; Yan, L. A Novel Multifunctional Photocatalytic Separation Membrane Based on Single-Component Seaweed-Like g-C_3N_4. *Adv. Funct. Mater.* **2023**, *33*, 2213974.
59. Xiao, Z.; Xiao, J.; Sun, Q.; Wang, Y.; Pan, L.; Shi, C.; Zhang, X.; Zou, J. J. Interface Engineering of Conjugated Polymer-Based Composites for Photocatalysis. *Chem. Eur. J.* **2022**, *28*, e202202593.